Fire Safety Journal 91 (2017) 864–871

Contents lists available at ScienceDirect

Fire Safety Journal

journal homepage: www.elsevier.com/locate/firesaf

IAFSS 12th Symposium 2017

Investigation of firebrand generation from an experimental fire: Development of a reliable data collection methodology

Jan C. Thomas[a], Eric V. Mueller[a], Simon Santamaria[a], Michael Gallagher[b], Mohamad El Houssami[a], Alexander Filkov[c,d], Kenneth Clark[b], Nicholas Skowronski[e], Rory M. Hadden[a,*], William Mell[f], Albert Simeoni[g]

[a] School of Engineering, University of Edinburgh, Edinburgh, UK
[b] Northern Research Station, USDA Forest Service, New Lisbon, NJ, USA
[c] School of Ecosystem and Forest Sciences, U. of Melbourne, Creswick, VIC 3363, Australia
[d] Tomsk State University, Department of Physical and Computational Mechanics, Russia
[e] Northern Research Station, USDA Forest Service, Morgantown, WV, USA
[f] Pacific Wildland Fire Science Lab, USDA Forest Service, Seattle, WA, USA
[g] Jensen Hughes, Inc., Framingham, MA, USA

ARTICLE INFO

Keywords:
Embers
Firebrand shower
Fire behavior
Wildfire
Forest fire
WUI

ABSTRACT

An experimental approach has been developed to quantify the characteristics and flux of firebrands during a management-scale wildfire in a pine-dominated ecosystem. By characterizing the local fire behavior and measuring the temporal and spatial variation in firebrand collection, the flux of firebrands has been related to the fire behavior for the first time. This linkage is seen as the first step in risk mitigation at the wildland urban interface (WUI). Data analyses allowed the evaluation of firebrand flux with respect to observed fire intensities for this ecosystem. Typical firebrand fluxes of 0.82–1.36 pcs m^{-2} s^{-1} were observed for fire intensities ranging between 7.35 ± 3.48 MW m^{-1} to 12.59 ± 5.87 MW m^{-1}. The experimental approach is shown to provide consistent experimental data, with small variations within the firebrand collection area. Particle size distributions show that small particles of area $0.75–5\times10^{-5}$ m^2 are the most abundant (0.6–1 pcs m^{-2} s^{-1}), with the total flux of particles $> 5\times10^{-5}$ m^2 equal to 0.2–0.3 pcs m^{-2} s^{-1}. The experimental method and the data gathered show substantial promise for future investigation and quantification of firebrand generation and consequently a better description of the firebrand risk at the WUI.

1. Introduction

Structures at the wildland urban interface (WUI) are particularly susceptible to ignition due to firebrand exposure [1,2]. Maranghides and Mell [3] outlined the need for a WUI-hazard scale assessment of the risks arising from wildfires and identified that direct fire and firebrand exposure are the leading cause of the ignition of structures in the WUI. Although there has been a considerable increase in the research activity in the area of firebrands and firebrand exposure in the last decade, no complete description of the problem yet exists. This challenge is compounded by the wide range of environmental and topographical conditions, ecosystems, and structure types that may be present during a WUI fire. Delivering understanding and solutions that are able to fit these diverse conditions continues to be a significant challenge for the fire science community. Most available studies related to firebrands have focused on characterizing the aerodynamics of typical firebrands [4] and analyzing the burning duration of firebrands [5,6] with respect to fire size and wind conditions [7]. Santamaria et al. [8] studied the impact of firebrand accumulation on ignition of wooden materials in inclined, V-shaped configurations. Spotting ignition from firebrands at short distance has been exhaustively investigated at laboratory scale by Manzello et al. [9–11]. Long-distance spotting (> 5 km) was described by Koo et al. [7]. A more detailed literature review, covering most studies related to firebrands and the exposure problem in the WUI, is presented by Caton et al. [1] and Hakes et al. [2].

This study focuses on the development of a methodology for characterizing the generation and flux of firebrands at short distance in large-scale fires, which can provide realistic input data for modelers and for laboratory-scale tests, in order to improve the resistance of WUI structures and communities to ember showers. Until now, there has been very little information available about the relationship between firebrand generation, fuel consumption, fire behavior and

* Corresponding author.

http://dx.doi.org/10.1016/j.firesaf.2017.04.002
Received 15 February 2017; Accepted 3 April 2017
Available online 19 April 2017
0379-7112/

Nomenclature

BW	black and white
DPT	Differential pressure transducer
FBP	fire behavior package
FCS	firebrand collection site
FMC	fuel moisture content (% dry weight)
I	fireline intensity (kW m^{-1})
L	flame length
LiDAR	light detection and ranging
PT	primary tower in FBP
PNR	Pinelands National Reserve
R (ROS)	fire rate of spread
ST	secondary tower in FBP
SD	standard deviation
TC	thermocouple
TSC	thin skin calorimeter
WNW	west-north-west
WUI	wildland-urban interface
X,Y,Z	locations
Δh_c	heat of combustion (kJ kg^{-1})
Δm	mass consumption (kg)

wind conditions, all combined in a real WUI fire or even in a large-scale field experiments. This understanding must come from detailed studies that cannot be achieved for large-scale wildfires, where accurate measurements are nearly impossible to carry out. For instance, very precise investigation work was carried out by Rissel et al. [12] and Manzello et al. [13] to characterize the size of the firebrands after a WUI fire, but they did not have access to a detailed description of fire behavior, making it impossible to link the firebrand generation to the fire.

The methodology used in this study is in alignment with a framework developed and presented in El Houssami et al. [14] and Filkov et al. [15], which reported integrated numbers of firebrands for local fire conditions and their characteristics (size, mass and origin). The novelty of this study includes the quantification of firebrand flux in time with respect to the local fire behavior, wind speed, fuel consumption, fire intensity, and characterizes the exposure of each sampling location. This information will help in estimating the firebrand flux that can be produced from a typical fire, the characteristics (geometry, mass) of the particles and if it is sufficient to impact a structure. This study falls in the configuration of low wind speed, flat terrain, and homogeneous fuel of the matrix suggested by Maranghides and Mell [3]. Since the methodology is developed with a full set of instruments to accurately measure the firebrands landing ahead of a fire front, it needs to first be tested in relatively controlled conditions at field scale, beginning with low wind speeds. Such a condition is not inherently a drawback for firebrand generation, because it was previously demonstrated that fire-induced drafts at low wind speeds were strong enough to detach bark pieces from tree boles and produce substantial amounts of firebrands [14]. Quantification of firebrand exposure in this way will allow a more complete description of the problem and allow the firebrand fluxes and characteristics to be linked to the fuels and fire behavior.

2. Experimental methods

2.1. Site description

This work was conducted in the Pinelands National Reserve (PNR) of New Jersey, USA. The region is characterized by a cool temperate climate, with a mean annual precipitation of 1160 mm and mean monthly temperatures ranging between 0 and 24 °C, from January to July. The terrain consists of plains, low-angle slopes, and wetlands, with a maximum elevation of 62.5 m. In the region of the study, the forest canopy is dominated by pitch pine (*Pinus rigida* Mill.), with intermittent oaks (*Quercus* spp.). Understory vegetation is composed of a mix of huckleberry (*Gaylussacia baccata*), blueberry (*Vaccinium palladum*), inkberry (*Ilex glabra*), briar (*Smilax rotundifolia*), scrub oak (*Quercus marilandica* and *Quercus ilicifolia*), wintergreen (*Gaultheria procumbens*), and sedge (*Carex pennsylvanica*), listed in relative order of importance. This general area is host to significant research activity, including studies on fire behavior [16] and firebrand generation [14], as well as a fuel management program directed by the New Jersey Forest Fire Service and federal wildland fire managers.

For this study, a burn parcel covering approximately 28 ha was selected, as shown in Fig. 1. The perimeter of the parcel was defined by existing access roads. The locations of measurement sites were first selected on the criteria that the collection of firebrands occur outside of the parcel, to avoid collection of falling debris, which can occur if the fire passes through a measurement site. This was an improvement on the methodology presented by El Houssami et al. [14]. The sites were then positioned based on a determination of the intended ignition pattern, depending on predicted wind conditions, in order to develop a head fire spreading towards the collection sites.

2.2. Fuel characterization

Pre- and post-burn measurements of the surface fuels (shrub and forest floor material) were taken at fifteen randomly selected destructive harvest locations. For each, a 0.5 m^2 area was harvested down to the mineral soil. Pre-burn sampling was conducted within the two weeks prior to the burns, and post-burn sampling was conducted within the following week. All shrub and forest floor materials present down to and excluding the duff layer were dried at 70 °C for a minimum of 48 h, sorted into different fuel classes and types, and weighed. The accuracy of destructive sampling is hindered by the fact that pre- and post-fire samples must inherently be collected in different locations. To handle this, the OpenBUGS (OpenBUGS, version 3.2.3 rev 1012) MCMC simulator11 was used to repeatedly resample and derive the distributional properties of the fuels from the harvested samples. Using these distributions, estimates of pre-burn loading, post-burn loading, and consumption were obtained. Note that standard hourly classifications of fuel diameter size are used here (1-hr: 0.0–6.35 mm; 10-hr: 6.35–25.4 mm).

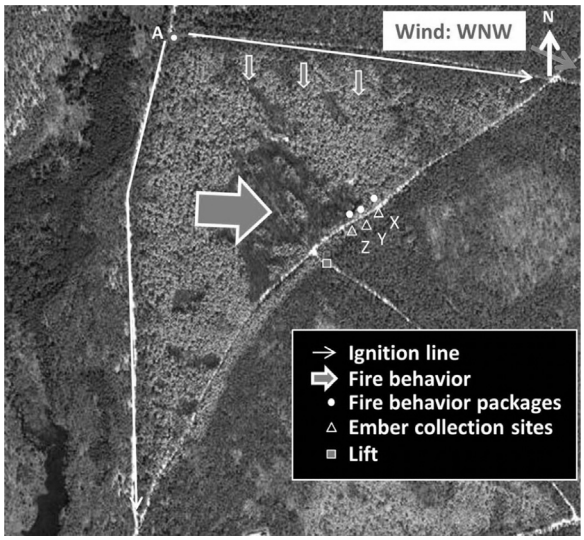

Fig. 1. Satellite image of burn unit (post fire). Indicating, general wind direction, ignition pattern, data collection package locations (Lift, FBP, FCS) and overall fire spread direction. The dark area in the middle of the image corresponds to an area of high consumption of canopy fuel.

Forest canopy biomass was estimated before and after treatments in 3 permanent 20×20 m plots, using a Riegl Laser Rangefinder (Model # LD90-3100VHS-FLP, Riegl USA, Orlando, FL). Following the methods described by Clark et al. [17] parallel transects spaced 1 m part were paced at a consistent rate with the LiDAR unit and logged to a Trimble Ranger. The device was carried at a height of 2 m, at the top of the shrub layer, providing canopy data above that height. Raw transect data was summarized into 1 m height bins across each plot, and were used to estimate available canopy fuel loading from the equation for pitch pine dominated stands in Clark et al. [17]. Available canopy fuels include live and dead needle, 1-hr, and 10-hr biomass.

Fuel moisture content (FMC), expressed as a percentage of water mass over oven dry mass, was estimated for surface and canopy fuel components. These included the forest floor, shrub, live pine needle, and live pine 1- and 10-hr twig material. Five samples of each component were harvested at the time of the burn, weighed wet, dried for 48 h at 70 °C, and weighed dry.

2.3. Fire behavior quantification

Meteorological conditions were monitored on a 17 m lift (located as shown in Fig. 1). This supported a 3D sonic anemometer (RM 80001 V, R. M. Young Co.) and a weather station. For the purpose of this study, the weather station was used to obtain averaged data of wind and temperature conditions.

Fire behavior was measured locally using a number of integrated sensors, positioned on two supporting towers for each site (Fig. 2e). Taken together, these sites are referred to as Fire Behavior Packages (FBP) (Figs. 1 and 2). The primary tower (6 m) supported six exposed K-Type thermocouples (sheath diameter of 250 μm), positioned at heights between 20–500 cm. The secondary tower (3.3 m) supported both bi-directional pressure probes for flow measurement [18] and thin-skin calorimeters (TSC) for heat flux measurement [19], as well as accompanying reference thermocouples for calibration purposes. All measurements were recorded at 50 Hz (CR3000, Campbell Scientific). Temperature measurements from the primary tower are considered here, and they are used to determine local flame height and spread rate. 27 video cameras were also positioned around the sites in fire proof boxes, at different heights and angles, in order to capture visual observations of the local fire behavior.

The energy release of the fire was quantified using the fireline intensity, I, the rate of energy release per unit length of fire front (kW m^{-1}). The first was by using a well-known method based on the rate of mass consumption [20]:

$$I = \Delta h_c \cdot \Delta m \cdot R, \quad (1)$$

where Δh_c is the low heat of combustion, taken as a general value for vegetative fuel of 18.7 MJ kg^{-1} [20], Δm is the mass consumed per unit area (kg m^{-2}), R is the rate of spread (m s^{-1}).

The second was by using a proposed empirical correlation between flame length and fireline intensity [20]:

$$I = 259.833 \cdot L^{2.174}, \quad (2)$$

where L is the flame length (m).

2.4. Firebrand collection

Firebrands were collected in circular aluminum cans (diameter: 22 cm, height: 12 cm) as depicted in Fig. 3. Cans were filled with a small amount water to extinguish the firebrands upon landing and to prevent them for being blown out by high wind gusts. After the experiment the water was drained from the cans, individual particles were separated. A standardized photo (Fig. 3) was taken of the inside of each can. Once the photos were taken, cans were left open to air dry particles for 24 h. The dried particles were collected and stored in a secure container. With this methodology it was not possible to distinguish between cold or hot particles or whether particles landed in smoldering of flaming state. All particles are reported as firebrands such that a conservative measurement of the firebrand flux is given.

2.4.1. Collection site

Firebrand Collection sites (FCS) were located outside the burn unit on the other side of the fuel break (dirt road, 3 m wide). The location was downwind of the fire determined by the anticipated fire behavior and ignition technique. For this experiment three FCS (X, Y and Z), were used. The location of each is indicated in Fig. 1. FCS Z was the most southern, X the most northern with Y in between. Separation distances from FBPs and FCSs are summarized in Table 1. An overhead image depicting the locations of FBP and FCSs is given in Fig. 4.

FCS X and Z are accompanied by a FBP as described above. The orientation of the FBP and FCS were selected according to the anticipated fire behavior. FCS and FBP alignment was determined based on forecast northerly winds (although the predominant wind direction varied from this). A typical FCS is shown in the photograph in Fig. 5 below. In addition to collections cans, a sonic anemometer was installed at a height of 3 m height to monitor wind conditions during the experiment. Several cameras were place around the plot to record visual observations.

Each FCS contained 50 water cans in which firebrands were collected. The FCS was laid out with three legs: left, center, right. The center leg was aligned with the FBP in the burn unit. Left and right legs were oriented with a 45° angle on the center sampling location. Each leg had two rows of cans. Each row had 8 (left/right) or 9 (center) cans. Cans were separated by a nominal distance of 0.5 m (in one row)

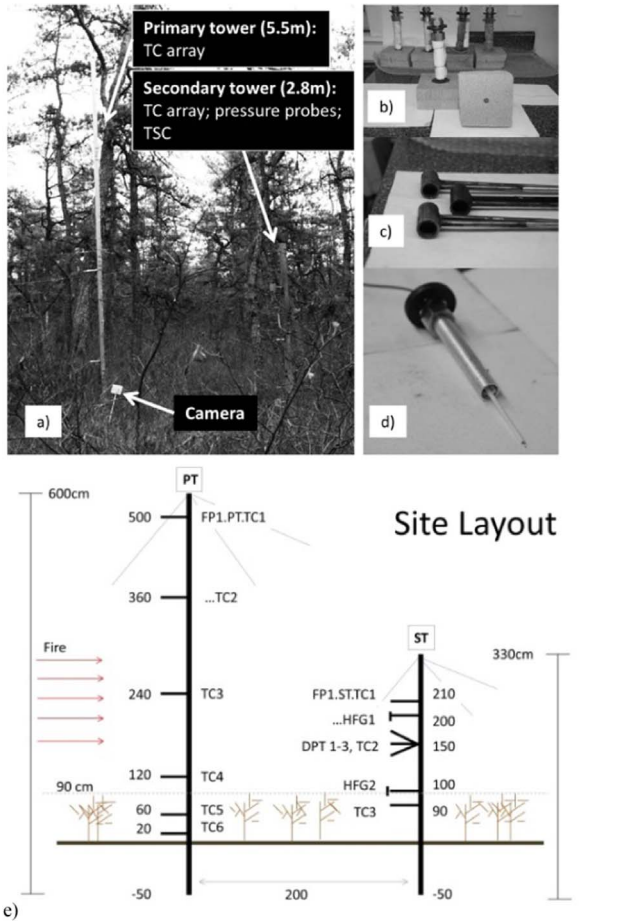

Fig. 2. (a) Photograph of a typical FBP setup, (b) thin skin calorimeter, (c) bi-direction pressure probes, (d) thermocouple assembly, and (e) FBP site layout (PT: primary tower, ST: secondary tower; units in [cm]).

Fig. 3. Standardized photograph of the inside of a typical aluminum firebrand collection can (diameter: 22 cm) with firebrands.

and each leg was approximately 4.5 m in length. The total area in which firebrands were collected was 1.83 m^2.

2.4.2. Video analysis

Several video cameras were positioned in the FCS to view the inside some of the cans in order to observe particles landing during the fire as a function of time (Fig. 6a). Post-fire analysis of the video footage allowed determination of the timing of important events, such as first and last firebrand arriving and the duration of the firebrand collection, which is required to determine a firebrand flux (e.g. [pcs m^{-2} s^{-1}]). Knowing the time frame in which firebrands are collected as well as the location of the fire front provides a means to correlate the firebrand flux to a separation distance and, subsequently, characteristics of fire behavior. This is crucial because the purpose of this project is to provide a methodology that allows the linkage of firebrand flux to a particular fire behavior.

2.4.3. Data analysis techniques

An image analysis program was developed to measure the projected area of particles from images taken of each pan [15]. Images were taken a constant distance from the pan using a platform as shown in Fig. 6b. A typical image of the inside of the can is presented in Fig. 3.

Images were cropped to analyze the inside of the can only. After cropping, the image was converted into a greyscale. Thresholding was then carried out by applying a black and white cutoff (BW cutoff) of pixel intensity to create a binary image. This was set manually to 0.6–0.65. To ensure consistency between images a fixed light source was used. A minimum particle size threshold of 7.5×10^{-6} m^2 was used to differentiate between the particles of interest and image artifacts. To verify the results from the image analysis, the program was run with varying size cutoffs until the number of particles counted by the program matched the number counted manually in a random selection of 10 cans.

A calibration of the pixel-to-area conversion factor and the BW cutoffs was made with a well-defined reference particle (US penny). The program was run with three BW cutoffs (0.88, 0.9, and 0.92) which gave an average pixel area of 32014 (± 1.89%). Using this and the known cross-section area of the reference particle, the pixel-to-area conversion factor was found to be 8.90×10^{-9} m^2 px^{-1}.

The image analysis provides (1) the total number [pcs] of firebrands per can and (2) the projected area [m^{-2}] of each firebrand per can. This data was processed to provide a firebrand flux [pcs m^{-2} s^{-1}] of firebrands per can, leg and FCS, using the area of the collection cans and the duration of the firebrand collection (assessed by video analysis).

Table 1
Separation distances [m] between FBPs and FCSs.

	FBP Z	FBP Y	FBP X
FCS Z	27	29	60
FCS Y	29	21	32
FCS X	58	40	20

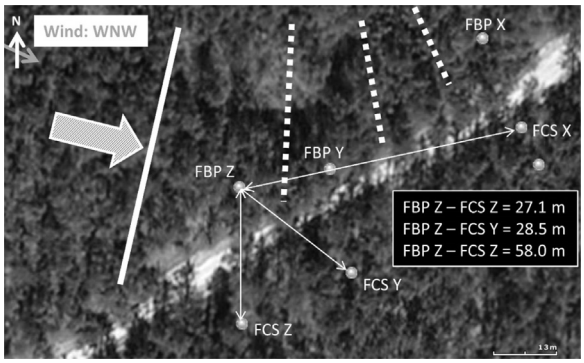

Fig. 4. Location of FBP and FCS with observed fire propagation (large arrow, solid and dotted lines).

3. Results and discussion

3.1. General features

The burn was conducted on March 18th, 2016, and ignition was at approximately 17:55 EST. During the burn period, mean ambient temperature was around 13 °C and mean relative humidity was 22%. The average wind speed was 1.4 ± 0.6 m/s (mean ± 1 SD) and the direction was WNW. Occasional gusts of up to 4.4 m/s were observed, as well as lulls of 0.5 m/s (1-min maximum and minimum values).

Ignition was carried out using drip-torches, with two simultaneous lines being drawn out along the north and west roads (starting from point A in Fig. 1), taking approximately 15 min to complete. The fire swept inward from the two roads, with the western portion turning somewhat, so that the fireline impacted the measurement areas from a west-northwesterly direction (Fig. 4). FBP Z was approached first. The northern ignition spread more slowly and with less intensity due to the non-alignment with the wind. Evidence of high intensity fire behavior in the center of the plot is given by the area of heavy consumption of canopy fuel seen in Fig. 1 (dark area in the middle of the image). The total burn was determined to last approximately 25–30 min.

FMC for all forest floor fuels and surface fuels were 31 ± 11%. For the canopy, pine needle and 1-h FMC were 122 ± 7%. The pre-burn, post-burn, and consumption values of the different fuel classes are given in Table 2. The LiDAR measurements provided an estimated a canopy height in the range 14–22 m.

3.2. Local fire behavior

A qualitative analysis of the video footage revealed that the fire approached FBP Z in a crowing state (Fig. 7a). As the fire travelled from Z to Y to X it reduced in intensity. At FBP X it was a moderate intensity shrub fire. Beyond FBP X, the fire continued to reduce until it burned out. This can also be seen in Fig. 7c, as plot X is just outside of the region of significant canopy fuel consumption.

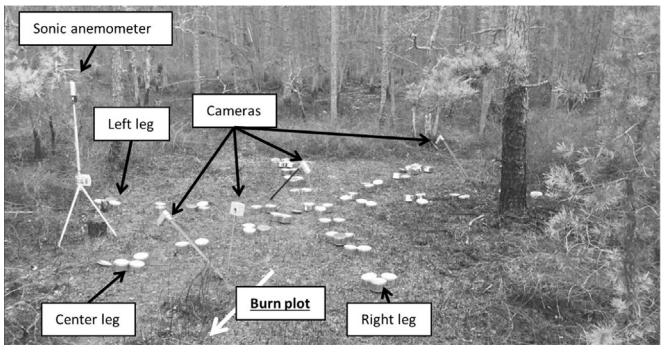

Fig. 5. Photograph of a typical FCS.

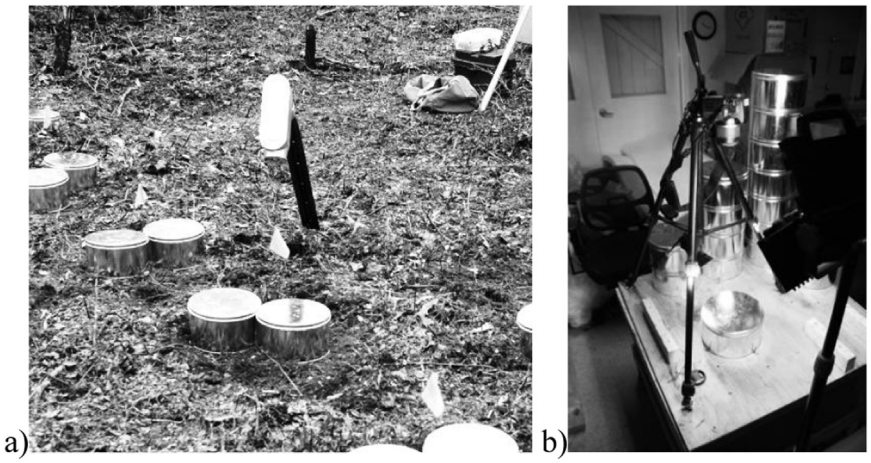

Fig. 6. (a) Close up of cans in FCS with camera protective housing above it; (b) Platform for standardized photography of cans.

Table 2
Average fuel consumption for the burn unit.

Fuel	Pre-burn [T ha^{-1}]	Post-burn [T ha^{-1}]	Consumption [T ha^{-1}]
Canopy (pitch pine)			
Pine needles, 1-hr, 10-hr	26.24 ± 0.88	16.48 ± 3.90	9.70 ± 8.72
Shrub fuel			
1-hr stems	5.35 ± 0.36	2.04 ± 1.19	3.31 ± 1.24
Forest floor			
Fine	13.94 ± 5.68	4.20 ± 2.50	9.74 ± 6.20
1-hr wood	1.31 ± 0.98	0.76 ± 0.64	0.55 ± 1.17

The rate of spread between FBP Z and FBP X was estimated by determining the fire arrival time (taken as the time of gas temperature exceeding 300 °C). From this, the fire was found to travel between the two sites in 197 s. With a separation of 57 m, this yielded a spread rate of 0.289 ± 0.014 m s^{-1} (considering a 5% uncertainty in the estimation of arrival time from the video). The average surface fuel consumption (forest floor and shrub material) was 1.36 ± 0.64 kg m^{-2} (Table 2). Using Eq. (1), a fireline intensity of 7.35 ± 3.48 MW m^{-1} is estimated, with the high variability coming from the variability in fuel consumption estimates (Table 2). This only considers surface fuel involvement, which video evidence (Fig. 7c) and aerial imagery (Fig. 1) suggest is representative of FBP X. However, FBP Z was on the edge of the region of significant canopy consumption, and adding the average contribution from this fuel (Table 2) gives a fire intensity of 12.59 ± 5.87 MW m^{-1}. This is 1.7 times the value for plot X. Note that the value should likely be on the upper end of this range (around 18 MW m^{-1}), as the parcel-wide average canopy consumption underestimates the peaks in such regions.

A quantification of the differences in fire behavior can also be made by examining the temperature measurements at the two sites (Fig. 8). Residence times were determined by identifying the first and last temperatures > 300 °C, using a 1-second moving average of the signals.

This temperature threshold is based upon observations for vegetative fuels [21]. From this, the flame intermittency can be determined at each height (Table 3), and the difference in flame characteristics can be seen between the two sites. Assuming that intermittencies below ~0.5 are above mean flame height, minimum mean flame heights of 2.4 m and 5.0 m are estimated for the two sites. These estimates are rough, and moving flames with fluctuating angles complicate the interpretation of intermittency, but the values are supported by video footage from the sites. If it is assumed that flame height is equivalent to flame length, Eq. (2) gives intensities of ~1.7 MW m^{-1} and 8.6 MW m^{-1} for FBP X and FBP Z, respectively. These, are lower than the values from Eq. (1), however, this variation can be accounted for by the variations in local fuel consumption, actual flame length, etc. Nevertheless, the temperature data serves to highlight the substantial difference in fire behavior over the distance between the two measurement sites.

3.3. Firebrand collection

Several firebrand collection results are discussed: (1) spatial variation in firebrand density within FCS, (2) duration of firebrand collection and timing of firebrand showers, (3) the total firebrand flux and (4) firebrand flux size distribution. A link between firebrand flux and fire exposure (separation and fire intensity) is made.

3.3.1. Spatial variability of firebrand collection

Fig. 9 shows typical firebrand collection data separated into each row of cans for FCS X (similar trends are seen for other sites). The firebrand density is the number of firebrands collected per unit area. Results indicate low variability between rows and legs. The firebrand density collected in two cans side by side has the same variability as cans separated by ~4.5 m (no clear trend was seen along the length of

Fig. 7. Still shots from video footage observing the fire behavior at each FBP: (a) fire is at FBP Z, (b) at FBP Y, and (c) at X. The camera in (a) and (b) is located just in front of FCS Y. The camera in (c) in front of FCS X. The line indicates the location of FBP in each site.

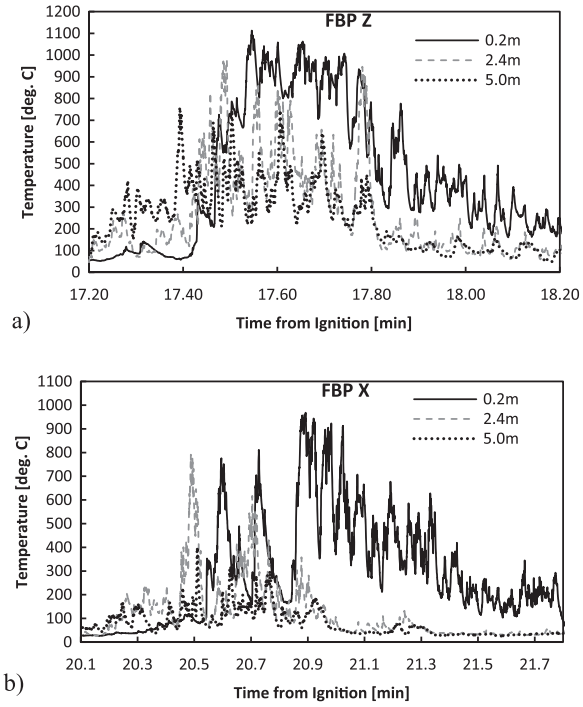

Fig. 8. Temperature evolution (PT) as the fire front passes through FBP Z (a) and X (b). For clarity, only three TCs measurements are shown here (6 total).

Table 3
Analysis of flame heights at FBP X and Z via flame intermittency.

TC ID (height from ground) [m]	Flame intermittency [-]					
	0.2	0.6	1.2	2.4	3.6	5.0
FBP X	0.75	0.45	0.44	0.46	0.18	0.00
FBP Z	0.85	0.71	0.99	0.88	0.67	0.69

each leg front to back either). This gives high confidence in the data collected.

3.3.2. Duration of collection and timing of firebrand showers

Video analysis provided information on the arrival of individual firebrands, from which it was possible to determine a duration of firebrand collection. Arrival time of firebrands is valuable information because it can be linked to the position of the fire front. In the analysis provided herein, it is assumed that the particles observed at a specific instant in the video analysis originated from the fire behavior at that time. Thus, it is assumed that the firebrand travel time is short ($t \rightarrow 0$ s). Although this is a strong assumption, analysis from previous studies [14] indicates that most firebrands travel relatively short distances. Estimation of the fire position based on the firebrand traveling in a straight line at the average wind speed suggests that an increase in travel distance on the order of 130%. While this may be significant for longer range firebrands, the absolute error resulting from short range firebrand showers is small. Improving this measurement further would require detailed knowledge of the exact origin and path of a given firebrand. A summary of events of interest is given in Table 4.

The arrival time of the first particles in FCS Z and FCS Y is very similar (5 min before fire front arrival at FBP Z), whereas, firebrands arrive slightly later at FCS X (4 min before fire front arrival at FBP Z). Separation distances are given in Table 1 and are shown in Fig. 4. It can be deduced that firebrand travel distances are significantly greater than 30 m in this fire (separation distances of FCS to FBP). It is possible to obtain a rough estimate of the fire front position at the time of the first

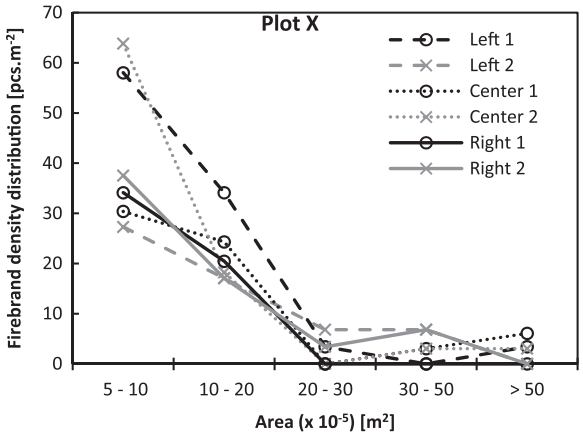

Fig. 9. Spatial variability of firebrand density distribution for FCS X. Each data series represents one row in the indicated leg.

firebrand arrival. For this, it is assumed that the ROS estimated earlier (0.289 m s^{-1}) is a characteristic value for this fire (in the area where it was calculated). In 5 min, the fire front travelled approximately 90 m. Therefore, at the time of arrival of first particle in FCS Z, the fire line was 90 m in front of the FBP Z. Thus, firebrand travelled in excess of 100 m before landing in the collection sites. This is likely an underestimation, since firebrand travel time is not considered, and the added time between generation and collection would imply an even greater separation distance at the time of generation.

A large flux of firebrands ('firebrand shower') was observed for approximately 1–2 min depending on the plot. These showers occurred at consecutive times from FCS Z to Y to X. This may be explained by the location of each plot in relation to the fire front movement. The firebrand showers for FCS Z and Y occurred at the time when the fire front was located around and after FBP Z. The separation distance of the FCS to the source (fire front) at the time of firebrand showers is consistently around 20–30 m for FCS Z and Y. Separation distance for FCS X is likely shorter, because it is closer to the fuel break.

The total duration of firebrand collection is, on average, 438 ± 65 s for each plot. The timing of firebrand collection is an important parameter because it allows the formulation of a firebrand flux [pcs m^{-2} s^{-1}] which can be used in WUI hazard assessments and laboratory studies, as explored below. The results obtained for this fire did not suggest any particular trends in collection time between FCS Z, Y and X, even though they had variation in fire exposure and separation distance. More experimentation is required to fully understand if there are any relations between fire behavior, separation distance and the time span of ember showers.

3.3.3. Total firebrand flux

The total firebrand flux is now calculated from the firebrand density, and the duration of firebrand collection in each FCS is summarized in Table 5.

A trends in the firebrand density and total firebrand flux can be observed, primarily that higher number fluxes of firebrands are present at sites with higher fire intensity. Two factors explain this trend: (1) fire intensity and (2) separation distance to source. FCS Z was exposed to

Table 4
Results of video analysis: first and last particle arriving, duration of firebrand collection, and timing of firebrand showers. Times are from ignition.

	FCS Z	FCS Y	FCS X
1st firebrand arriving [mm: ss]	12:13	12:50	13:24
Firebrand showers [mm: ss]	16:38–18:40	17:53–19:00	18:05–19:37
Last firebrand arriving [mm: ss]	18:47	20:23	19:11
Duration of collection [s]	394	513	407

Table 5
Firebrand collection analysis: firebrand density, duration of collection and total firebrand flux.

	FCS Z	FCS Y	FCS X
Firebrand density [pcs m^{-2}]	536	463	335
Time span [s]	394	513	407
Total firebrand flux [pcs m^{-2} s^{-1}]	1.361	0.902	0.824

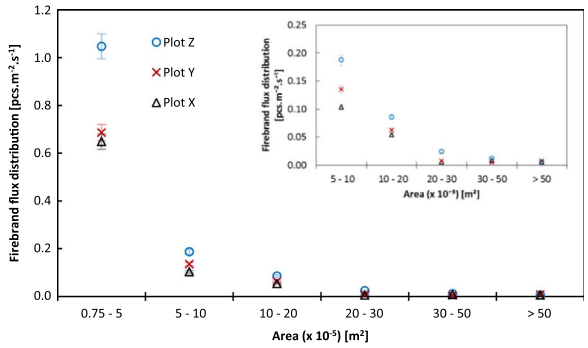

Fig. 10. Firebrand flux size distribution for all FCSs. The inlay provides more detail on the largest size classes (error bars: standard 5% error due to temporal uncertainty).

the highest flux, X to the lowest and Y mid-range. These results reflect the changes in fire behavior discussed above (fire traveling from FBP Z to X and with decaying intensity). Therefore, it can be deduced that FCS Z had a higher exposure compared to X. The firebrand flux was reduced by 39% from FCS Z to X. Similarly, the fire intensity was reduced by 40% from FBP Z to X (using averaged values from Eq. (2) estimates). Although a significant correlation would be premature, these data analyses show the linkage between realistic wildfire behavior and firebrand generation.

3.3.4. Firebrand flux distribution

The total firebrand flux cannot distinguish between particle size, which is desirable information to have in order to fully characterize risks associated with a firebrand shower. The total size distribution of the firebrand flux for each FCS is shown in Fig. 10. The size classes were chosen according to [14,15], with one additional group, capturing fine particles ($0.75–5\times10^{-5}$ m^2) due to the high number of particles in this size range that were deemed as not ash.

Similar to observations from the total firebrand flux, a variation in the size distribution can also be identified. The flux for low and medium size particles ($\leq30\times10^{-5}$ m^2) is highest for FCS Z and lowest for X. As was discussed above, FCS Z has the highest exposure from the fire due to its proximity to the most intense fire behavior. As the separation distance to the most intense fire behavior increases from Z to Y to X, the flux distribution decreases. As the fire moves closer towards FCS Y and X it decreases in intensity, generating fewer firebrands. More detailed characterization of the firebrand flux is given in Table 6.

The percent reduction of the flux from FCS Z to Y and X is relatively consistent for particles $< 20\times10^{-5}$ m^2. For each size category the flux reduces 28–34% from Z to Y and 37–45% from Z to X It is more variable for larger particles, however, since few particles of this size are collected it is difficult to draw definitive conclusions.

4. Conclusions

This study presents a novel and reliable methodology for collecting firebrands from field-scale fires in order to characterize typical firebrand fluxes. The goal was to provide fundamental insight into firebrand generation and quantify the risk of firebrand exposure as a function of fire behavior. This will aid fire risk assessments in the WUI and provide experimental data to assess firebrand generation in model

Table 6
Firebrand collection analysis: Firebrand flux size distribution.

Size group [m^2]	Flux distribution [pcs m^{-2} s^{-1}]			Reduction from FCS Z [%]	
	FCS Z	FCS Y	FCS X	FCS Y	FCS X
0.75–5 ($\times10^{-5}$)	1.0473	0.6858	0.6483	34	38
5–10	0.1873	0.1352	0.1034	28	45
10–20	0.0856	0.0618	0.0537	28	37
20–30	0.0236	0.0075	0.0054	68	77
30–50	0.0118	0.0043	0.0081	64	32
> 50	0.0059	0.0075	0.0054	–26	9

applications. Although firebrands have been collected and characterized in previous studies (field and laboratory), this work presents advances in quantifying firebrand flux data with a correlation to the observed fire behavior.

The data analysis described allowed the quantification of relevant fire behavior (rate of spread and intensity) and firebrand flux [pcs m^{-2} s^{-1}]. The local rate of spread was 0.289 ± 0.014 m s^{-1}. Fire intensity was estimated between 7.35 ± 3.48 MW m^{-1} to 12.59 ± 5.87 MW m^{-1} depending on the location. Total firebrand flux was estimated between 0.824 and 1.361 pcs m^{-2} s^{-1} depending on the location of collection and the associated fire behavior. The collection area with highest firebrand flux was correlated to the highest fire intensity and the lowest flux to the lowest fire intensity. Visual observations coupled with fire behavior measurements showed that periods of high intensity firebrand showers occurred up to 100 m ahead of the fire front. At greater separation distances, lower particle fluxes were observed.

The presented methodology resulted in usable and reliable outcomes with a high level of consistency. The remaining challenge in applying this methodology to real wildfires is understanding the required fire behavior measurements. Future development of this methodology should address the following issues which have been identified: (1) deployment of a larger sensor network to quantify fire behavior over the relevant distances; (2) improved firebrand flux resolution data with visual observations; (3) improved assumptions of firebrand transport time; and (4) improved assessment of separation distance between firebrand showers and fire front. Improvements in these areas will provide a step forward in the causes and quantification of firebrand generation and consequently improve hazard assessment for WUI communities.

Acknowledgments

The authors would like to thank the Joint Fire Science Program (JFSP) for their financial support under the project grant #15-01-04–55. Many thanks to the NJ Forest Fire Service without whom the field experiment would not have been possible. Dr. Filkov was supported by The Tomsk State University Academic D.I. Mendeleev Fund Program.

References

[1] S.E. Caton, R.S.P. Hakes, D.J. Gorham, A. Zhou, M.J. Gollner, Review of pathways for building fire spread in the wildland urban interface Part I: exposure conditions, Fire Technol. (2016).
[2] R.S.P. Hakes, S.E. Caton, D.J. Gorham, M.J. Gollner, A review of pathways for building fire spread in the wildland urban interface Part II: response of components and systems and mitigation strategies in the United States, Fire Technol. (2016).
[3] A. Maranghides, W. Mell, Framework for Addressing the National Wildland Urban Interface Fire Problem - Determining Fire and Firebrand Exposure Zones Using a WUI Hazard Scale. Technical Note 1748, Gaithersburg, MD, 2012.
[4] P.F. Ellis, The aerodynamic and combustion characteristics of eucalypt bark—a firebrand study, Ph.D. Dissertation, Australian National University, Canberra, 2000.
[5] C.S. Tarifa, P.P. del Notario, F.G. Moreno, On the flight paths and lifetimes of burning particles of wood, Symp. (Int.) Combust. 10 (1) (1965) 1021–1037.

[6] F.A. Albini, Spot Fire Distance from Burning Trees - A Predictive Model, Ogden, Utah, 1979.
[7] E. Koo, P.J. Pagni, D.R. Weise, J.P. Woycheese, Firebrands and spotting ignition in large-scale fires, Int. J. Wildland Fire 19 (2010) 818–843.
[8] S. Santamaria, K. Kempna, J.C. Thomas, M. El Houssami, E. Mueller, D. Kasimov, A. Filkov, M.R. Gallagher, N. Skowronski, R. Hadden, A. Simeoni, Investigation of structural wood ignition by firebrand accumulation. in: Proceedings of the First international conference on structures safety under fire blast. Glasgow, UK, pp 1–13, 2015.
[9] S.L. Manzello, T.G. Cleary, J.R. Shields, J.C. Yang, On the ignition of fuel beds by firebrands, Fire Mater. 30 (2006) 77–87.
[10] S.L. Manzello, J.R. Shields, T.G. Cleary, A. Maranghides, W.E. Mell, J.C. Yang, Y. Hayashi, D. Nii, T. Kurita, On the development and characterization of a firebrand generator, Fire Saf. J. 43 (2008) 258–268.
[11] S.L. Manzello, S. Suzuki, Y. Hayashi, Enabling the study of structure vulnerabilities to ignition from wind driven firebrand showers: a summary of experimental results, Fire Saf. J. 54 (2012) 181–196.
[12] S. Rissel, K. Ridenour, Ember production During the Bastrop complex fire, Fire Manag. Today 72 (4) (2013).
[13] S.L. Manzello, E.I.D. Foote, Characterizing Firebrand Exposure from Wildland–Urban Interface (WUI) Fires: results from the 2007 Angora Fire, Fire Technol. 50 (2014) 105–124.
[14] M. El Houssami, E. Mueller, A. Filkov, J.C. Thomas, N. Skowronski, M.R. Gallagher, K. Clark, R. Kremens, A. Simeoni, Experimental procedures characterising firebrand generation in wildland fires, Fire Technol. 52 (3) (2016) 731–751.
[15] A. Filkov, S. Prohanov, E. Mueller, D. Kasymov, P. Martynov, M. El Houssami, J. Thomas, N. Skowronski, B. Butler, M. Gallagher, K. Clark, W. Mell, R. Kremens, R.M. Hadden, A. Simeoni, Investigation of firebrand production during prescribed fires conducted in a pine forest, Proc. Combust. Inst. (2016) 1–8.
[16] E.V. Mueller, N.S. Skowronski, K.L. Clark, R. Kremens, M.R. Gallagher, J.C. Thomas, M. El Houssami, A. Filkov, B. Butler, J. Hom, W.E. Mell, A. Simeoni, An experimental approach to the evaluation of prescribed fire behavior, *Proceedings of the VII International Conference on Forest Fire Research*, 2014, pp. 41–53.
[17] K.L. Clark, N.S. Skowronski, M. Gallagher, N. Carlo, M. Farrell, M.R. Maghirang, Assessment of canopy fuel loading across a heterogeneous landscape using lidar, Jt. Fire Sci. Program (2013) 47 (Final Report 10-1-02-14).
[18] B.J. McCaffrey, G. Heskestadt, A robust bidirectional low-velocity probe for flame and fire application, Combust. Flames 26 (1979) (127-127).
[19] ASTM E 459-05, Standard Test Method for Measuring Heat Transfer Rate Using a Thin-Skin Calorimeter, ASTM International, West Conshohocken, PA, 2016.
[20] M.E. Alexander, M.G. Cruz, Interdependencies between flame length and fireline intensity in predicting crown fire initiation and crown scorch height, Int. J. Wildland Fire 21 (2012) 95–113.
[21] A.L. Sullivan, P.F. Ellis, I.K. Knight, A review of radiant heat flux models used in bushfire applications, Int. J. Wildland Fire 12 (2003) 101–110. http://dx.doi.org/10.1071/WF02052.